Tests des Standardmodells der Teilchenphysik

Spezialfach Kern-Teilchen-Astrophysik

Tests of the Standard Model of Particles

Spring Semester 2018

Lecture 7

Dr. Zinonas Zinonos
zinonos@mpp.mpg.de

Max-Planck-Institut für Physik, TUM

June 7, 2018

Overview

The Drell-Yann process

The W-boson mass and quantum loop corrections

The top quark

Top quark decay

Top quark mass

Top quark cross section

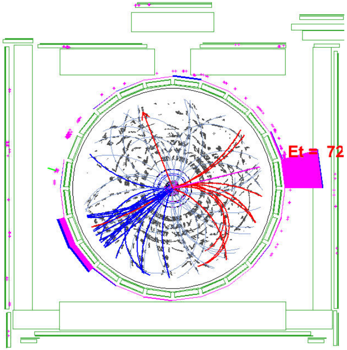

Figure 1: Single-top event candidate at CDF with an electron.

The Drell-Yann process

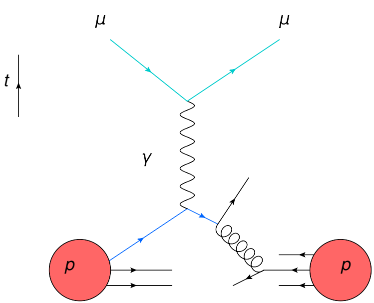

Figure 2: Feynman diagram for the Drell–Yan process $pp \to \mu^+\mu^- + \text{jet(s)}$.

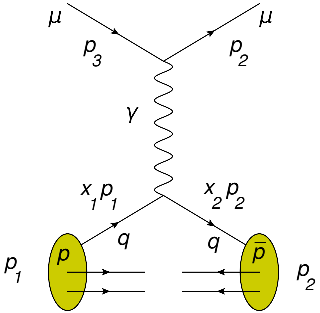

Figure 3: The lowest-order Feynman diagram for the Drell–Yan process $p\bar{p} \to \mu^+\mu^- + \text{jet(s)}$.

The Drell-Yan process occurs in high energy hadron–hadron scattering and takes place when a quark of one hadron and an antiquark of another hadron annihilate, creating a virtual photon or Z boson which then decays into a pair of oppositely-charged leptons.

A useful example of a $pp \to \mu^+\mu^-$ cross section calculation for hadron–hadron collisions.

We calculated the QED annihilation cross section for $e^+e^- \to \mu^+\mu^-$ in lecture 7 of SM I,

$$\sigma(e^+e^- \to \mu^+\mu^-) = \frac{4\pi\alpha^2}{3s} \tag{1}$$

The corresponding cross section for $q\bar{q} \to \mu^+\mu^-$ annihilation is

$$\sigma(q\bar{q} \to \mu^+\mu^-) = \frac{Q_q^2}{N_c}\frac{4\pi\alpha^2}{3\hat{s}} \tag{2}$$

where

- Q_q is the quark/antiquark electric charge
- $\hat{s}$ is the center-of-mass energy of the colliding $q\bar{q}$ system
- the factor N_c^{-1} with $N_c = 3$ is the number of colors.

The factor N_x accounts for the conservation of colour charge $\longrightarrow$ implies that of the 9 possible color combinations of the $q\bar{q}$ system, the annihilation process can only occur for three, $r\bar{r}$, $b\bar{b}$ and $g\bar{g}$.

The contribution to the overall Drell–Yan cross section from an *up*-quark within the proton with momentum fraction $x_1 \to x_1 + \delta x_1$ annihilating with an *anti-up*-quark within the other proton with momentum fraction $x_2 \to x_2 + \delta x_2$ is

$$d^2\sigma = Q_u^2 \frac{4\pi\alpha^2}{9\hat{s}} u(x_1)dx_1\, \bar{u}(x_2)dx_2 \tag{3}$$

where $u(x_i)$ is the PDF for the quark i in the colliding proton and likewise $\bar{u}(x_i)$ for the antiquark of the other proton (or antiproton).

However, the antiquark PDFs within the antiproton or the other proton, will be identical to the corresponding quark PDFs in the proton

$$\bar{u}(x_i) = u(x_i) \tag{4}$$

we can write

$$d^2\sigma = \left(\frac{2}{3}\right)^2 \frac{4\pi\alpha^2}{9\hat{s}} u(x_1)dx_1\, u(x_2)dx_2 \tag{5}$$

The center-of-mass energy of the quark-antiquark pair, each carrying 4-momentum p_i, $i = 1, 2$ can be expressed in terms of that of the proton-(anti)proton system using

$$\hat{s} = (x_1 p_1 + x_2 p_2)^2 = x_1^2 p_1^2 + x_2^2 p_2^2 + 2x_1 x_2 p_1 \cdot p_2 \tag{6}$$

In the high-energy limit, $E \gg m$, the proton mass squared can be neglected

$$p_1^2 = p_2^2 \approx 0 \quad \longleftrightarrow s = (p_1 + p_2)^2 \simeq 2p_1 p_2 \tag{7}$$

and thus

$$\hat{s} \simeq x_1 x_2 (2p_1 p_2) = x_1 x_2 s \tag{8}$$

where s is center-of-mass energy of the colliding pp system. Therefore, Eq. (6) can be expressed in terms of s as

$$d^2\sigma = \frac{4}{9} \frac{4\pi\alpha^2}{9x_1 x_2 s} u(x_1) u(x_2) dx_1 dx_2 \tag{9}$$

In the case of proton-antiproton collisions, we must account for the smallercontribution from the annihilation of a $\bar{u}$-quark in the proton with a u-quark in the antiproton. In addition we need to consider the contribution from $d\bar{d}$ annihilation.

This will lead to an expression for the differential cross section of

$$d^2\sigma = \frac{4\pi\alpha^2}{9x_1x_2s} f(x_1,\, x_2) \tag{10}$$

with

$$f(x_1,\, x_2) = \left[\frac{4}{9}\left(u(x_1)u(x_2) + \bar{u}(x_1)\bar{u}(x_2)\right) + \frac{1}{9}\left(d(x_1)d(x_2) + \bar{d}(x_1)\bar{d}(x_2)\right)\right] \tag{11}$$

The Drell–Yan differential cross section can be expressed in terms of the experimental observables for more useful interpretations

A suitable choice is the rapidity y and the invariant mass of the $\mu^+\mu^-$ system. Both observables can be determined from the momenta of the final state muons as reconstructed by the detector.

The invariant mass of the dimuon system is equal to the center-of-mass energy of the colliding partons

$$M^2 \equiv m_{\mu\mu}^2 = x_1 x_2 s \tag{12}$$

The rapidity of the muon-pair is given by

$$y = \frac{1}{2} \ln \frac{E_3 + p_3^z + E_4 + p_4^z}{E_3 - p_3^z + E_4 - p_4^z} = \frac{1}{2} \ln \frac{E_q + p_q^z + E_{\bar{q}} + p_{\bar{q}}^z}{E_q - p_q^z + E_{\bar{q}} - p_{\bar{q}}^z} \tag{13}$$

where 3 labels the quark q and 4 labels the antiquark $\bar{q}$.

The equality of four-momenta of the dimuon system and that of the colliding partons following from energy and momentum conservation suggests that the four-momentum of the colliding q is

$$p_q = x_1 p_1 = (x_1 E_1,\, 0,\, 0,\, x_1 p_1) = \frac{\sqrt{s}}{2}(x_1,\, 0,\, 0,\, x_1) \tag{14}$$

assuming $E = |p|$ in the limit $E \gg m$ and knowing that

$$E_{\text{com}} = \sqrt{s} = 2 x_i E_i \quad (i = 1,\, 2) \tag{15}$$

Likewise, the four-momenta of the colliding $\bar{q}$ is given by

$$p_{\bar{q}} = \frac{\sqrt{s}}{2}(x_2,\, 0,\, 0,\, -x_2) \tag{16}$$

since the incoming partons collide with equal and opposite-sign momenta $\boldsymbol{p}_1 = -\boldsymbol{p}_2$.

Therefore,

$$y = \frac{1}{2}\ln\frac{x_1 + x_1 + x_2 - x_2}{x_1 - x_1 + x_2 - (-x_2)} = \frac{1}{2}\ln\frac{x_1}{x_2} \Rightarrow \frac{x_1}{x_2} = e^{2y} \tag{17}$$

Combined the above expression with (12), we find for x_1 and x_2 in terms of $m_{\mu\mu}$ and y

$$x_1 = \frac{M}{\sqrt{s}}e^{y} \qquad x_2 = \frac{M}{\sqrt{s}}e^{-y} \tag{18}$$

The differential cross section in terms of $dx_1\, dx_2$ can be expressed in terms of $dy\, dM$ using the determinant of the Jacobian matrix $J(x_1,\, x_2)$ for the coordinate transformation

$$dy\, dM = \frac{\partial(y,\, M)}{\partial(x_1,\, x_2)}\, dx_1\, dx_2 = \begin{vmatrix} \partial y/\partial x_1 & \partial y/\partial x_2 \\ \partial M/\partial x_1 & \partial M/\partial x_2 \end{vmatrix} dx_1\, dx_2 \tag{19}$$

$$= \frac{s}{2M} dx_1\, dx_2 \tag{20}$$

Consequently, the differential cross section of (6) can be expressed as

$$d^2\sigma = \frac{4\pi\alpha^2}{9M^2} f(x_1,\, x_2)\frac{2M}{s} dy\, dM \tag{21}$$

and thus, the Drell–Yan differential cross section, written in terms of the invariant mass M and rapidity y of the dimuon system is

$$\frac{d^2\sigma}{dy\,dM} = \frac{8\pi\alpha^2}{9Ms} f(x_1,\, x_2) \tag{22}$$

with momentum fractions x_i given by (18).

The previous treatment of the Drell–Yan process considered exclusively the QED γ-exchange diagram. However, any neutral boson which couples to both quarks and muons can contribute to this process, for example the Z boson.

The next figure shows the measured differ ential cross section for $p\bar{p} \to \mu^+\mu^- + X$ from the CDF experiment at the Tevatron.

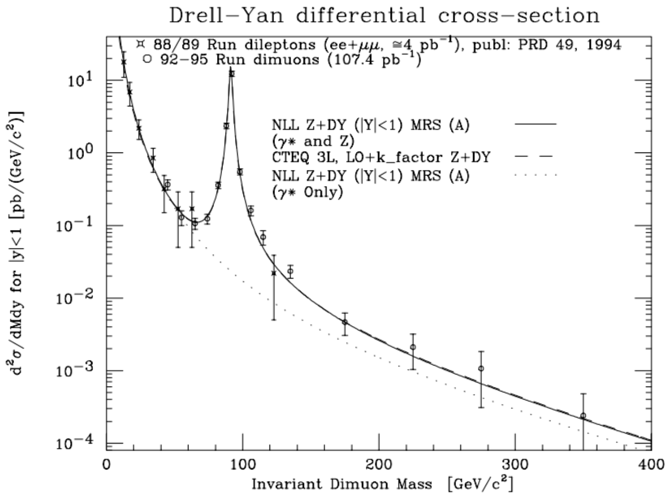

Figure 4: Feynman diagram for the Drell–Yan process $pp \to \mu^+\mu^- +$ jet(s).

Drell-Yan dimuon production cross section extracted from the combined 1992-1993 and 1994-1995 CDF data at Tevatron. The solid line is the NLO QCD prediction. The dashed line is the LO QCD prediction with a k-factor to account for higher order effects. The dotted line is the NLO QCD prediction without the contribution from Z^0 exchange. Ref.: Phys.Rev. D59 (1999) 052002.

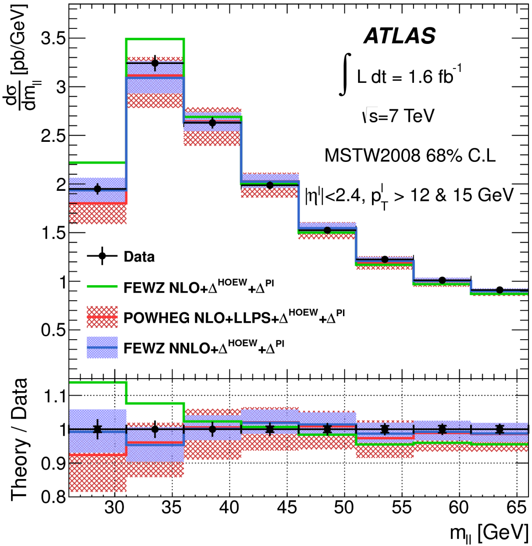

Ref.: ATLAS, 2014, arXiv:1404.1212.

Measured differential cross section, $d\sigma/dm_{\ell\ell}$ after selection cuts as a function of the invariant mass $m_{\ell\ell}$ (solid points) compared to NLO predictions.

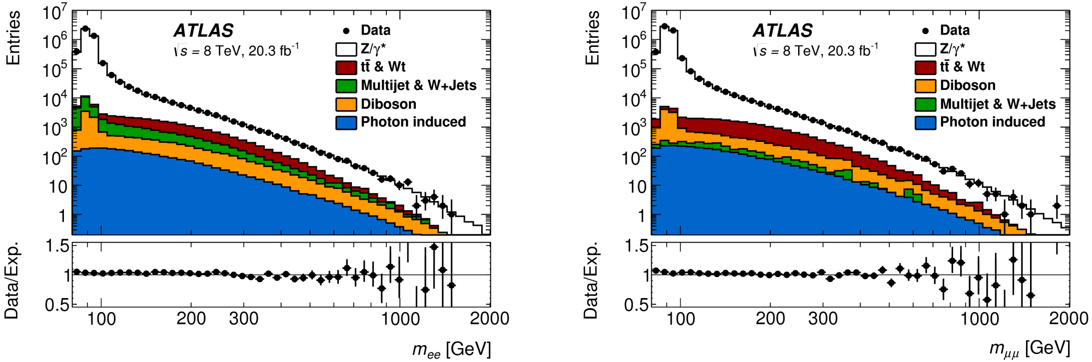

The invariant di-lepton (high) mass distribution after event selection for the electron selection (left) and muon selection (right), shown for data (solid points) compared to the expectation (stacked histogram). The lower panels show the ratio of data with its statistical uncertainty to the expectation. Ref.: ATLAS, 2014, arXiv:1606.01736.

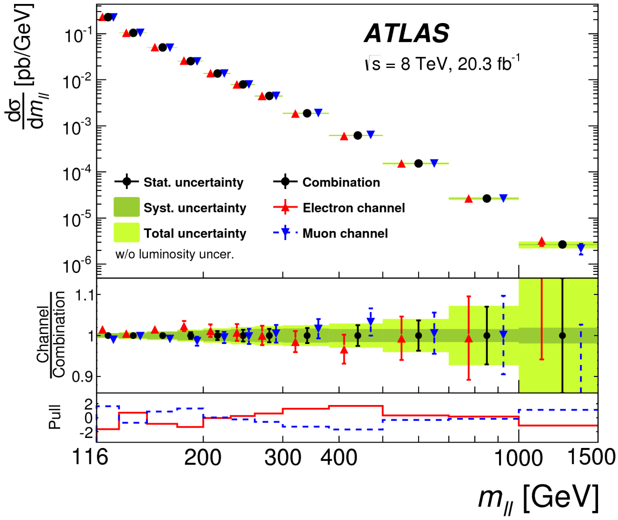

Ref.: ATLAS, 2014, arXiv:1606.01736.

Comparison of the electron, muon and combined (black points) single-differential fiducial Born-level cross sections as a function of invariant (high) mass $m_{\ell\ell}$. The error bars represent the statistical uncertainty. The inner shaded band represents the systematic uncertainty on the combined cross sections, and the outer shaded band represents the total measurement uncertainty (excluding the luminosity uncertainty). The central panel shows the ratio of each measurement channel to the combined data, and the lower panel shows the pull of the electron and muon channel measurements with respect to the combined data.

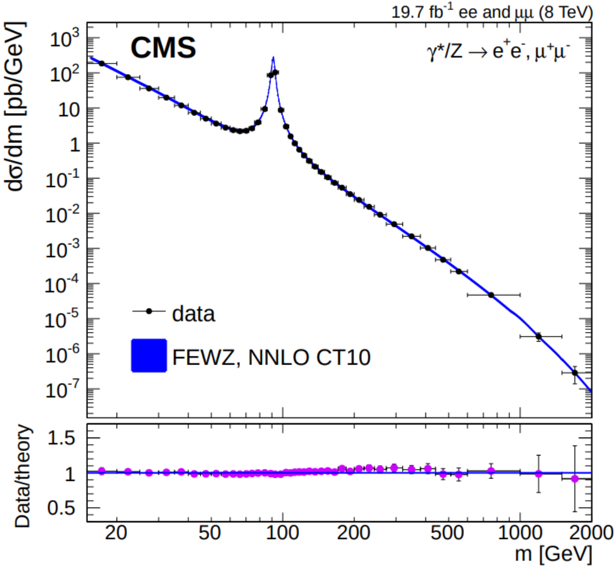

Ref.: CMS, 2015, arXiv:1412.1115.

The DY differential cross section as measured in the combined dilepton channel at $\sqrt{s} = 8\ \mathrm{TeV}$ and as predicted at NNLO with CT10 PDF calculations, for the full phase space.

The Drell–Yan process also provides a tool of searching for physics beyond the Standard Model through the production of new massive neutral particles that couple to both quarks and leptons, through the process $q\bar{q} \xrightarrow{X^0} \ell^+\ell^-$.

Models with extended gauge groups often feature additional $U(1)$ symmetries with corresponding heavy spin-1 bosons. These bosons, generally referred to as Z', would manifest as a narrow resonance through its decay, in the dilepton mass spectrum.

Among these models are those inspired by Grand Unified Theories, which are motivated by gauge unification or a restoration of the left-right symmetry violated by the weak interaction.

Another example is the Sequential Standard Model (SSM) which manifests a Z'_{SSM} boson with couplings to fermions equal to those of the SM Z boson.

$\rightsquigarrow$ To date, no such signals of physics beyond the Standard Model have been observed.

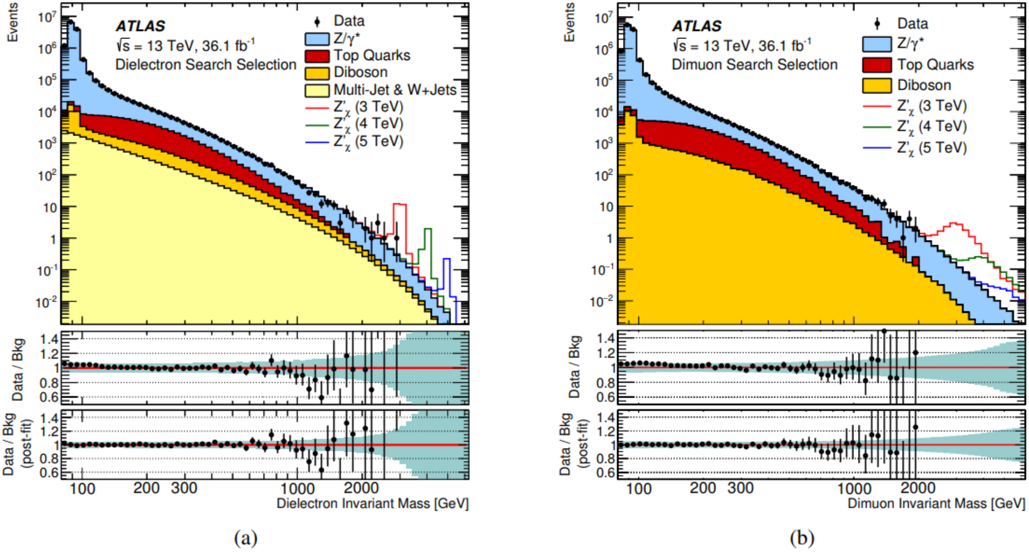

Figure 5: : Distributions of (a) dielectron and (b) dimuon reconstructed invariant mass ($m_{\ell\ell}$) after selection, for data and the SM background estimates. ATLAS, 2017, arXiv:1707.02424v2.

W-boson mass measurement

We have seen in lecture 12 of SM I, that the study of W-boson pair production at LEP provides precise measurements of m_W, Γ_W and the W-boson branching ratios.

Precision measurements can also be conducted at hadron colliders. For example, m_W can be measured precisely at the Tevatron in the process $p\bar{p} \to W + X$, where X is the hadronic system from initial-state QCD radiation and the remnants of the colliding hadrons, and at LHC in the process $pp \to W + X$.

In proton-(anti)proton collisions, the W boson is produced in parton-level processes such as $u\bar{d} \xrightarrow{W^+} \mu^+ \bar{\nu}_\mu$.

The reconstruction the mass of the W boson, m_W requires a precise determination of the momentum of the produced neutrino which leads to the E_T^{miss} in the event.

As discussed before, at hadron colliders, the center-of-mass energy of the underlying $q\bar{q}$ annihilation process is not known on an event-by-event basis.

Therefore, the four-momentum of the final state can be written as

$$p_1 = \left(x_1 \frac{\sqrt{s}}{2},\ 0,\ 0,\ +x_1 \frac{\sqrt{s}}{2}\right) \tag{23}$$

$$p_2 = \left(x_2 \frac{\sqrt{s}}{2},\ 0,\ 0,\ -x_2 \frac{\sqrt{s}}{2}\right) \tag{24}$$

$$\Rightarrow p_{\text{tot}} = \frac{\sqrt{s}}{2}\,(x_1 + x_2,\ 0,\ 0,\ x_1 - x_2) \tag{25}$$

This implies that, the final-state W boson will be boosted along the beam (z) axis.

Because the momentum fractions x_1 and x_2 are unknown, the components of the momentum of the final-state system only balance in the transverse (x-y) plane.

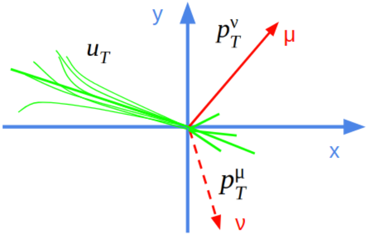

Typical $W \to \mu\nu$ event topology, as observed in the plane transverse to the beam axis.

The transverse components of the neutrino momentum, $\boldsymbol{p}_T(\nu)$,can be reconstructed from the transverse momentum of the muon, $\boldsymbol{p}_T(\mu) = (p_x,\, p_y)$ and the transverse momentum $\bar{u}_T$ of the hadronic system X that recoils the W-boson decay,

$$\boldsymbol{p}_T(\nu) + \boldsymbol{p}_T(\mu) + \boldsymbol{u}_T = 0 \tag{26}$$

with $E_T^{\mathrm{miss}} = |\boldsymbol{p}_T^{\nu}|$. The z-component of the neutrino momentum cannot be determined since the momentum fractions of the colliding partons are unknown.

Therefore, the invariant mass of the products from the decaying W boson can not be determined on an event-by-event-basis.

However, it is possible to define the transverse mass of the W boson as

$$\begin{aligned} m_T &= \sqrt{2\left(p_T(\mu) p_T(\nu) - \boldsymbol{p}_T(\mu) \cdot \boldsymbol{p}_T(\nu)\right)} \quad (27)\\ &= \sqrt{2 p_T(\mu) E_T^{\mathrm{miss}} \left(1 - \cos\Delta\phi(\mu,\, E_T^{\mathrm{miss}})\right)} \quad (28) \end{aligned}$$

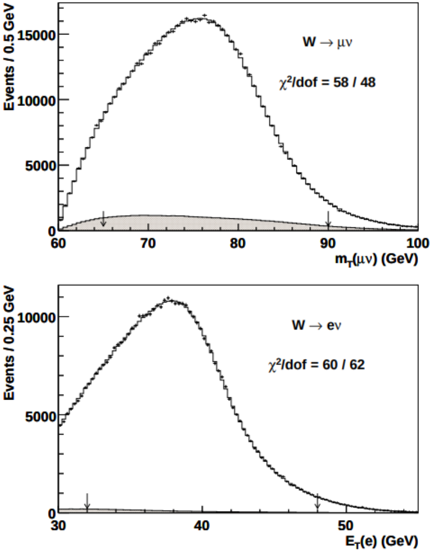

Figure 6: Measurements of the W-boson mass by the LEP and Tevatron experiments.

The m_T distribution for muons (top) and the p_T^ℓ distribution for electrons (bottom) as measured by the CDF experiment.

The data (points) and the best-fit simulation template (histogram) including backgrounds (shaded) are shown. Ref.: arXiv:1203.0275.

Because the longitudinal components of the momentum are not included, m_T does not peak at m_W and the distribution of m_T is relatively broad.

Nevertheless, these disadvantages are outweighed by the generally very large W-production cross section at hadron-hadron colliders.

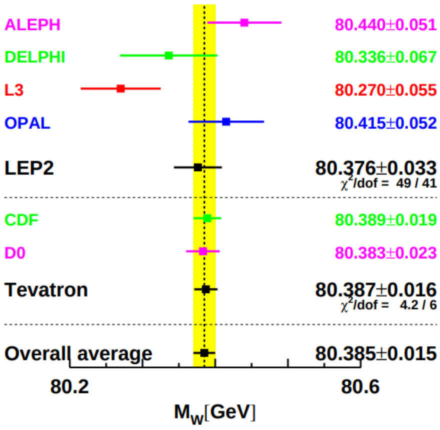

Figure 7: Measurements of the W-boson mass by the LEP and Tevatron experiments.

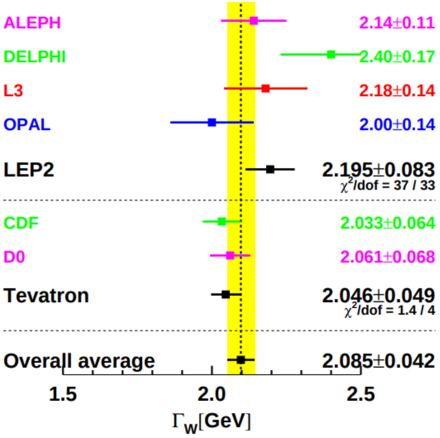

Figure 8: Measurements of the W-boson width by the LEP and Tevatron experiments.

Ref.: PDG review, 2015.

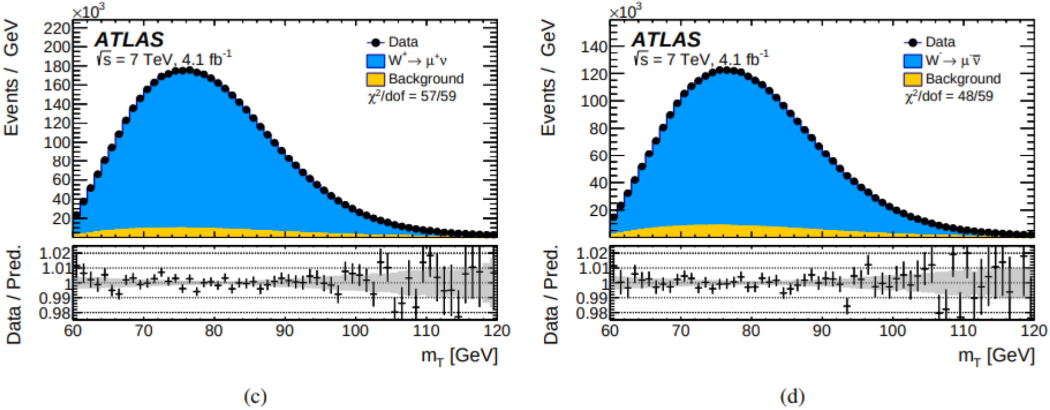

Figure 9: The m_T distribution in $W^+ \to \mu^+\nu$ and $W^- \to \mu^-\bar{\nu}$ as measured by the ATLAS collaboration at $\sqrt{s} = 7$ TeV. Ref.: ATLAS 2017, arXiv:1701.07240v1

Because of the large numbers of events, m_W can be measured even more precisely at LHC than at LEP. The sensitivity to m_W comes from the shape of the m_T distribution and the position of the broad peak.

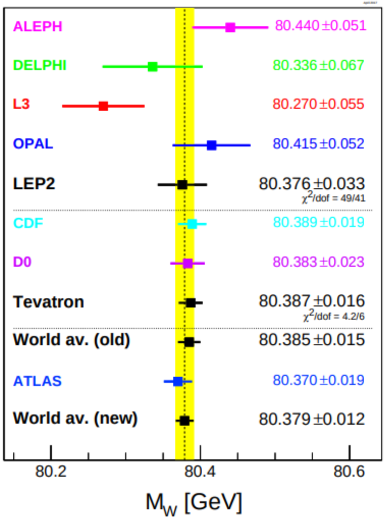

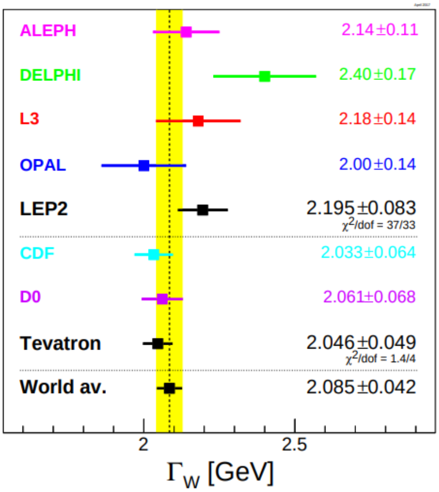

Measurements of the W-boson mass and width by the LEP, Tevatron and LHC experiments: The combination (Ref.: PDG review, 2015.) gives

$$\boxed{m_W = 80.379 \pm 0.012 \text{ GeV} \quad \Gamma_W = 2.085 \pm 0.042 \text{ GeV}}$$

W mass determination overview

Hadron colliders

Production of on-shell W bosons at hadron colliders is tagged by the high p_T charged lepton from its decay. Owing to the unknown parton-parton effective energy and missing energy in the longitudinal direction, the collider experiments reconstruct the transverse mass of the W, m_T, and derive the W mass from comparing the transverse mass distribution with Monte Carlo predictions as a function of m_W. These analyses use the electron and muon decay modes of the W boson.

e^+e^- colliders

AT LEP a precise knowledge of the beam energy enables one to determine the $e^+e^- \to W^+W^-W$ cross section as a function of center of mass energy, $\sqrt{s}$, as well as to reconstruct the W mass precisely from its decay products, even if one of them decays leptonically. Close to the WW threshold (161 GeV), the dependence of the W-pair production cross section on m_W is large, and this was used to determine m_W. At higher energies (172 to 209 GeV) this dependence is much weaker and W-bosons were directly reconstructed and the mass determined as the invariant mass of its decay products, improving the resolution with a kinematic fit.

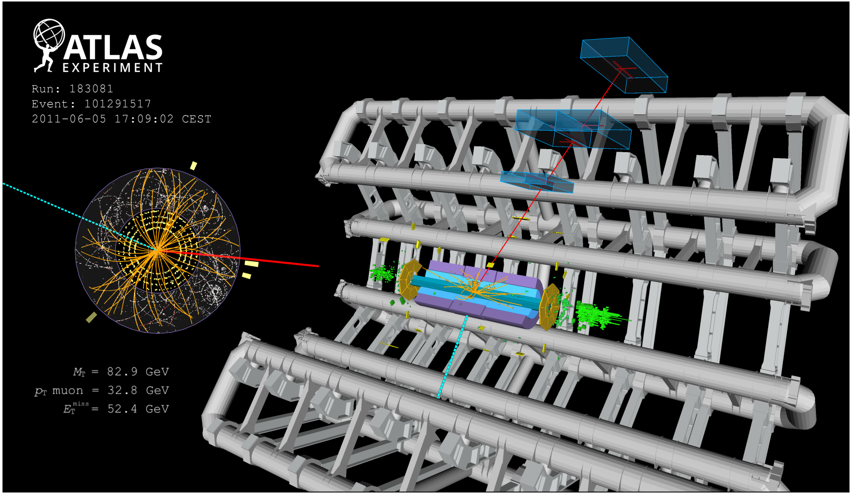

Display of a candidate event for a W boson decaying into one muon and neutrino from pp collisions recorded by ATLAS with LHC stable beams at a collision energy of 7 TeV. The muon (red line) has a transverse momentum of 32.8 GeV and the missing transverse energy is 52.4 GeV (cyan blue line), resulting in a transverse mass of 82.9 GeV of the di-lepton system. Little hadronic activity is measured, indicating a small transverse momentum of the W boson candidate. The event was recorded in June 2011 and was used for the measurement of m_W.

Quantum loop corrections

In the Standard Model, the masses of the W and Z bosons are not free parameters, they are determined by the Higgs mechanism, described in lecture 15 of SM I.

Consequently, if any three of the parameters

$$m_Z,\, m_W,\, G_F,\, \alpha, \sin^2\theta_W \tag{29}$$

are known, the other two are determined by exact relations from the electroweak unification mechanism of the Standard Model.

For example, the mass of the W boson is related to α, G_F and θ_W by

$$\frac{G_F}{\sqrt{2}} = \frac{g_W^2}{8m_W^2},\, g_W^2 = 4\pi\alpha_W,\, \alpha = \alpha_W \sin^2\theta_W \Rightarrow m_W = \sqrt{\frac{\pi\alpha}{\sqrt{2}G_F}\frac{1}{\sin^2\theta_W}} \tag{30}$$

with

$$G_F = 1.1663787(6)^{-5} \text{ GeV}^{-2} \tag{31}$$

$$\alpha(m_Z^2) = \frac{1}{128.91 \pm 0.02} \tag{32}$$

$$\sin^2\theta_W = 0.23146 \pm 0.00012 \quad \text{(weak mixing angle)} \tag{33}$$

and the masses of the W and Z bosons being related by

$$m_W = m_Z \cos\theta_W \tag{34}$$

Using the measurements of $\sin^2\theta_W$ and Z boson mass

$$m_Z = 91.1875 \pm 0.0021 \text{ GeV} \ , \tag{35}$$

the predicted mass of the W boson obtained from (34) is

$$m_W^{\text{pred}} = 79.937 \pm 0.009 \text{ GeV} \tag{36}$$

Despite being of the right order of the predicted value, the prediction undershoots the experimental measurement of (24) by $\sim 30\sigma$!

Fortunately, this apparent discrepancy between theory and experiment does not represent a fatal failure of the Standard Model in predicting the W-boson mass.

Higher-order contributions from virtual quantum loop corrections explain the discrepancy. For example, the propagator the W boson includes contributions from virtual loops, of which the two largest are shown below

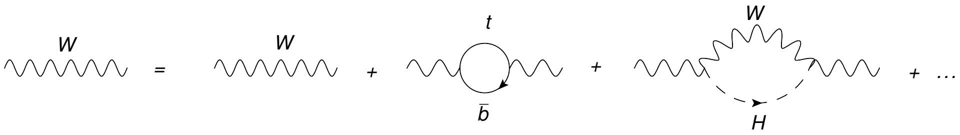

Figure 10: Lowest-order radiative corrections to the W mass involving top and bottom quarks and the Higgs.

Considering the quantum loop corrections, the physical W-boson mass differs from the lowest-order prediction m_W^0 by

$$m_W = m_W^0 + c_0 m_t^2 + c_1 \ln \frac{m_H}{m_W} + \ldots \tag{37}$$

where c_0 and c_1 are calculable constants, and m_t and m_H are the masses of the top quark and Higgs boson, respectively.

Since the dependence on the Higgs mass is only logarithmic, the dominant correction comes from the top quark mass.

The measurements of the electroweak parameters at LEP in 1994 implied a top quark mass of $175 \pm 11\ \mathrm{GeV}$. Shortly afterwards, the top quark was discovered at the Tevatron with a mass consistent with the prediction by LEP.

► The direct observation of the effects of quantum loop corrections provided an impressive confirmation of the electroweak sector of the Standard Model.

► Any new particle or interaction that gives rise to a significant contribution to the quantum loop corrections to the W-boson mass would immediately spoil the consistency with the experimental data $\rightarrowtail$ precision measurements with sensitivity to quantum loop corrections, they strongly constrain possible models for physics beyond the Standard Model!

The top quark

In the Standard Model (SM), the left-handed (LH) top quark is the $Q = 2/3$, $I_3 = +1/2$ member of the weak-isospin doublet containing the bottom quark, while the right-handed (RH) top is an $SU(2)_L$ singlet.

Its phenomenology is driven by its large mass; it is the most massive fundamental particle in the Standard Model,

$$m(t) > m(H) > m(Z) > m(W) \tag{38}$$

Being heavier than the W boson, it is the only quark that decays semi-weakly, i.e. into a real W boson and a b quark. Because $|V_{tb}| \gg |V_{ts}| > |V_{td}|$, the top quark decays almost entirely by $t \to b\,W^+$.

It has a very short lifetime and decays before hadronization can occur. Consequently, the top pairs produced in the process $q\bar{q} \to t\bar{t}$ do not have time to form bound states, such as those observed in the resonant production of charmonium ($c\bar{c}$) and bottomonium ($b\bar{b}$) states.

In addition, it is the only quark whose Yukawa coupling to the Higgs boson is order of unity

$$\sqrt{2}\frac{m_t}{v} \sim 1 \tag{39}$$

For these reasons, the top quark plays a special role in the Standard Model and in many extensions thereof.

Its phenomenology provides a unique laboratory where our understanding of the strong interactions, both in the perturbative and non-perturbative regimes, can be tested

Because of its mass, the top quark could not be observed directly at LEP and was only discovered in 1994 in $p\bar{p}$ collisions at the Tevatron.

In hadron collisions, top quarks are produced dominantly in pairs through the processes $q\bar{q} \to t\bar{t}$ and $gg \to t\bar{t}$, at leading order in QCD.

Approximately 85% of the production cross section at the Tevatron ($p\bar{p}$ at 1.96 TeV) is from $q\bar{q}$ annihilation, with the remainder from gluon-gluon fusion.

At LHC (pp) about 90% of the production is from gluon-gluon fusion at $\sqrt{s} = 14\ \mathrm{TeV}$ and $\sim 80\%$ at $\sqrt{s} = 7\ \mathrm{TeV}$.

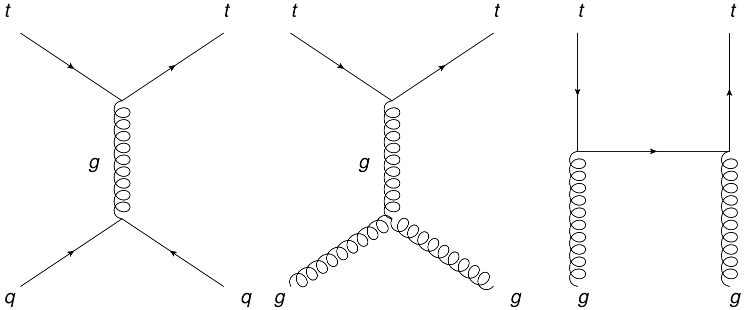

Figure 11: Lowest-order Feynman diagram for $t\bar{t}$ production in pp or $p\bar{p}$ collisions.

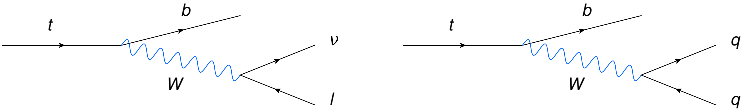

Figure 12: Top quark decay $t \to W^+b$ where the W boson can decay either leptonically or hadronically.

The corresponding matrix element contains four propagators for massive particles; two for the top quarks and two for the W bosons.

Because $\Gamma_W \ll m_W$, the largest contributions to the matrix element will be when the W bosons are produced almost on-shell with $q^2 \sim m_W^2$.

Similarly, the presence of the propagators for the two virtual top quarks implies that

$$|\mathcal{M}|^2 \propto \frac{1}{(q_1^2 - m_t^2)^2 + m_t^2\Gamma_t^2} \times \frac{1}{(q_2^2 - m_t^2)^2 + m_t^2\Gamma_t^2} \tag{40}$$

As a result, the invariant masses of each of the W^+b and W^-b systems stemming from the $t\bar{t}$ decay, will be distributed according Lorentzian centered on m_t with width Γ_t.

Top quark decay

Because the W boson from the decay of a top quark is close to being on-shell, $q^2 \sim m_W^2$, the top decay width can be calculated from the Feynman diagram for the decay $t \to b\, W^+$.

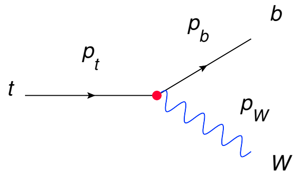

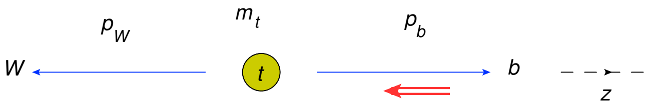

With a mass above the Wb threshold, and $|V_{tb}| \gg |V_{td}|, |V_{ts}|$, the decay width of the top quark is expected to be dominated by the two-body channel $t \to b\, W^+$.

The corresponding matrix element can be obtained from the quark spinors, the weak charged-current vertex factor and the polarization term of the involved W boson,

$$
\begin{aligned}
i\mathcal{M} &= \bar{u}(p_b)\frac{-ig_W}{\sqrt{2}}\gamma^\mu \tfrac{1}{2}(1-\gamma^5)u(p_t)\ \epsilon^*_\mu(p_W) && (41)\\
&= \frac{-ig_W}{\sqrt{2}}\bar{u}(p_b)\tfrac{1}{2}(1-\gamma^5)u(p_t)\ \epsilon^*_\mu(p_W) && (42)
\end{aligned}
$$

Considering the decay in the rest frame of the top quark and neglecting the mass of the b-quark, the four-momenta of the involved particles can be written as

$$
\begin{aligned}
p_t &= (m_t,\,0,\,0,\,0) && (43)\\
p_b &= (p,\,0,\,0,\,+p) \quad \text{with} \quad p = |p| && (44)\\
p_W &= (E,\,0,\,0,\,-p) && (45)\\
& && (46)
\end{aligned}
$$

with p being the magnitude of the momentum of the final-state particles in the center-of-mass frame and E is the energy of the W boson in the same reference

$$E^2 = p^2 + m_W^2 \qquad (47)$$

The weak interaction couples only to LH chiral particle states.

In the high-energy limit $p \gg m_b$, the chiral states are equivalent to the helicity states and thus the b-quark can only be produced in a LH helicity state.

Therefore, the spin configuration of Fig. 12 points in the negative z-direction.

Having this in mind, the matrix element can be written as

$$\mathcal{M} = -\frac{g_W}{\sqrt{2}} \bar{u}_\downarrow(p_b)\gamma^\mu u(p_t)\epsilon^*_\mu(p_W) \tag{48}$$

From lecture 5 of SM I, we found that the LH helicity spinor for the b-quark is

$$u_\downarrow(p_b) = \sqrt{p}\begin{pmatrix} 0 \\ 1 \\ 0 \\ -1 \end{pmatrix} \tag{49}$$

For the top quark at rest, $E = m_t \Rightarrow E + m_t = 2m_t$, there are two possible spin states which can be expressed as (see Appendix IV)

$$u_1(p_t) = \sqrt{2m_t}\begin{pmatrix}1\\0\\0\\0\end{pmatrix} \quad \text{represents} \quad \hat{S}_z = +\frac{1}{2} \tag{50}$$

$$u_2(p_t) = \sqrt{2m_t}\begin{pmatrix}0\\1\\0\\0\end{pmatrix} \quad \text{represents} \quad \hat{S}_z = -\frac{1}{2} \tag{51}$$

The four-vector quark currents for the two possible spin states for top, calculated using the relations shown lecture 10 of SM I

$$j_1^\mu = \bar{u}_\downarrow(p_b)\gamma^\mu u_1(p_t) = \sqrt{2m_t p}\ (0,\ -1,\ -i,\ 0) \tag{52}$$

$$j_2^\mu = \bar{u}_\downarrow(p_b)\gamma^\mu u_2(p_t) = \sqrt{2m_t p}\ (1,\ 0,\ 0,\ 1) \tag{53}$$

(See about γ matrices in Appendix V).

The three possible polarization states of the W boson are (see Appendix VI),

$$\epsilon_{+}^{\mu *}(p_W) = -\frac{1}{\sqrt{2}}(0,\, +1,\, -i,\, 0) \quad \text{with} \quad \hat{S}_Z = +1 \tag{54}$$

$$\epsilon_{L}^{\mu *}(p_W) = +\frac{1}{m_W}(-p,\, 0,\, 0,\, E) \quad \text{with} \quad \hat{S}_Z = 0 \tag{55}$$

$$\epsilon_{-}^{\mu *}(p_W) = +\frac{1}{\sqrt{2}}(0,\, +1,\, +i,\, 0) \quad \text{with} \quad \hat{S}_Z = -1 \tag{56}$$

For a particular top quark spin configuration and W boson polarization state, the matrix element of (48) can be given by the four-vector scalar product

$$\mathcal{M}_k = -\frac{g_W}{\sqrt{2}} j_{i\,\mu} \cdot \epsilon_{\lambda}^{\mu *} \quad \text{for} \quad i = 1,\, 2 \quad \text{and} \quad \lambda = +,\, -,\, 0 \tag{57}$$

Among of the possible combinations of two possible quark currents and the three possible W-boson polarizations, the matrix element is non-zero for

$$\epsilon_{+}^{*} \cdot j_1 \quad \text{and} \quad \epsilon_{L}^{*} \cdot j_2 \tag{58}$$

These two non-vanishing combinations correspond to the spin states shown below

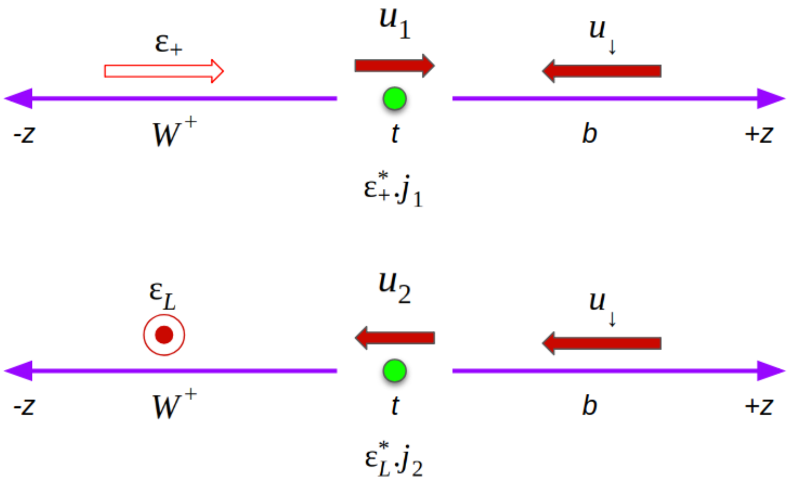

which are the only configurations that conserve angular momentum.

The matrix elements for the two allowed spin configurations are

$$
\begin{aligned}
\mathcal{M}_1 &= -\frac{g_W}{\sqrt{2}} j_{1\,\mu} \cdot \epsilon_+^{\mu *} = -\frac{g_W}{\sqrt{2}} \sqrt{2 m_t p}\ (0,\ -1,\ -i,\ 0)\ \frac{-1}{\sqrt{2}} (0,\ +1,\ -i,\ 0) && (59)\\
&= +g_W \sqrt{2 m_t p} && (60)\\
\mathcal{M}_2 &= -\frac{g_W}{\sqrt{2}} j_{2\,\mu} \cdot \epsilon_L^{\mu *} = -\frac{g_W}{\sqrt{2}} \sqrt{2 m_t p}\ (1,\ 0,\ 0,\ 1)\ \frac{1}{m_W} (-p,\ 0,\ 0,\ E) && (61)\\
&= +\frac{g_W}{m_W} \sqrt{m_t p}\, (p + E) && (62)\\
&= +\frac{g_W}{m_W} \sqrt{m_t p}\, m_t \quad \text{from energy-momentum conservation} \quad E + p = m_t && (63)\\
&= +g_W \frac{m_W}{m_t} \sqrt{m_t p} && (64)
\end{aligned}
$$

Therefore, the spin-averaged matrix element squared for the decay $t \to bW^+$ is

$$
\left\langle |\mathcal{M}|^2 \right\rangle = \sum_{\text{t spins}} = \frac{1}{2} |\mathcal{M}|^2 = \frac{1}{2} \left(|\mathcal{M}_1|^2 + |\mathcal{M}_2|^2 \right) \tag{65}
$$

where the factor of $1/2$ averages over the two possible spin states of the t-quark.

We then find

$$\left\langle |\mathcal{M}|^2 \right\rangle = \tfrac{1}{2} g_W^2 m_t p \left(2 + \frac{m_t^2}{m_W^2}\right) \quad \checkmark \tag{66}$$

The total decay rate is obtained by substituting the spin-averaged matrix element into the general formula (see lecture 3 of SM I) for 2-body decays $1 \to 2 + 3$

$$\Gamma = \frac{p}{32\pi^2 m_1^2} \int |\mathcal{M}|^2 \, d\Omega = \frac{p}{32\pi^2 m_1^2} 4\pi \, |\mathcal{M}|^2 \quad \text{(isotropic decay)} \tag{67}$$

where p is the magnitude of the momentum of either of the final-state particles in the rest frame of the decaying particle. Plugging in the matrix element squared and integrating over the 4π solid angle we find

$$\Gamma(t \to bW^+) = \frac{g_W^2 p^2}{16\pi m_t} \left(2 + \frac{m_t^2}{m_W^2}\right) \quad \text{with} \quad \frac{G_F}{\sqrt{2}} = \frac{g_W^2}{8 m_W^2} \tag{68}$$

$$= \frac{G_F}{2\sqrt{2}\pi} \frac{m_W^2 p^2}{m_t} \left(2 + \frac{m_t^2}{m_W^2}\right) \tag{69}$$

$$= \frac{G_F}{2\sqrt{2}\pi} p^2 m_t \left(1 + 2\frac{m_W^2}{m_t^2}\right) \tag{70}$$

From energy-momentum conservation of (43)-(45) we find

$$p_W = p_b - p_t \xrightarrow{\square} p_W^2 = p_b^2 + p_t^2 - 2p_b \cdot p_t \tag{71}$$

$$|\boldsymbol{p}| = \frac{m_t}{2}\left(1 - \frac{m_W^2}{m_t^2}\right) \tag{72}$$

and after some minimum algebraic manipulation we find

$$\Gamma(t \to bW^+) = \frac{G_F m_t^3}{8\sqrt{2}\pi}\left(1 - \frac{m_W^2}{m_t^2}\right)^2 \left(1 + 2\frac{m_W^2}{m_t^2}\right) \quad \checkmark \tag{73}$$

Considering the QCD corrections and neglecting terms of order

$$\frac{m_b^2}{m_t^2}, \quad \alpha_s^2 \quad \text{and} \quad \frac{\alpha_s}{\pi}\frac{m_W^2}{m_t^2} \tag{74}$$

the width predicted in the SM at NLO is

$$\Gamma(t \to bW^+) = \frac{G_F m_t^3}{8\sqrt{2}\pi}\left(1 - \frac{m_W^2}{m_t^2}\right)^2 \left(1 + 2\frac{m_W^2}{m_t^2}\right)\left[1 - \frac{2\alpha_s}{3\pi}\left(\frac{2\pi^2}{3} - \frac{5}{2}\right)\right] \tag{75}$$

where m_t refers to the top-quark pole mass.

The width for

- $m_t = 173.3`\text{GeV}$
- $m_W = 80.4\ \text{GeV}$
- $G_F = 1.166 \times 10^{-5}\ \text{GeV}^{-2}$
- $\alpha_s(m_Z) \simeq 0.118$

is

$$\boxed{\Gamma_t = 1.35\ \text{GeV}} \tag{76}$$

and increases with mass. Therefore, its lifetime is

$$\tau_t \equiv \frac{1}{\Gamma_t} = 5 \times 10^{-25}\text{s} \tag{77}$$

which is sufficiently short that the top quarks produced a hadron colliders decay in a distance of order $0.1\ \text{fm}$.

This is small compared to the typical length scale for the hadronization process, and therefore the $t\bar{t}$ pairs produced only decay before top-flavored hadrons or $t\bar{t}$-quarkonium-bound states are formed, but also decay before hadronizing.

This important feature allows physicists to observe "bare" top quarks.

Measurement of the top quark mass

The mass of the top quark has been firstly measured in the process $p\bar{p} \to t\bar{t}$ by direct reconstruction of the top quark decay products.

Since both top quarks decay to a b-quark and a W boson there are three distinct final-state topologies:

	process	signature	branching ratio
	$bq_1\bar{q}_2\ \bar{b}q_3\bar{q}_4$	6 jets	45.7%
$t\bar{t} \to (bW^+)(\bar{b}W^-) \to$	$bq_1\bar{q}_2\ \bar{b}\ell^-\bar{\nu}_\ell$	4 jets, 1 charged lepton, 1 neutrino	43.8%
	$b\ell^+\nu_\ell 2\ \bar{b}\ell'^-\bar{\nu}_{\ell'}$	2 jets, 2 charged leptons, 2 neutrinos	10.5%

The quarks in the final state evolve into jets of hadrons. The above processes are referred to as

1. fully-hadronic,
2. semi-leptonic, or, semi-hadronic
3. fully-leptonic

channels, respectively.

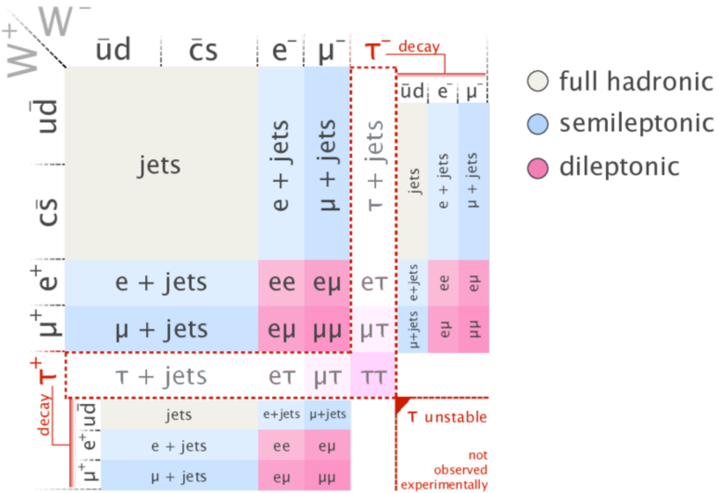

Possible final states of the decay of a top-quark pair.

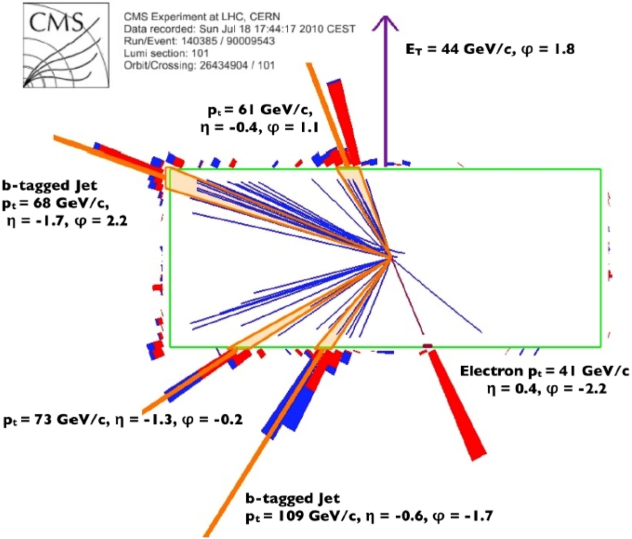

A $t\bar{t}$ event candidate with four jets, an electron, two b-tagged jets, and large missing transverse energy recored by the CMS detector.

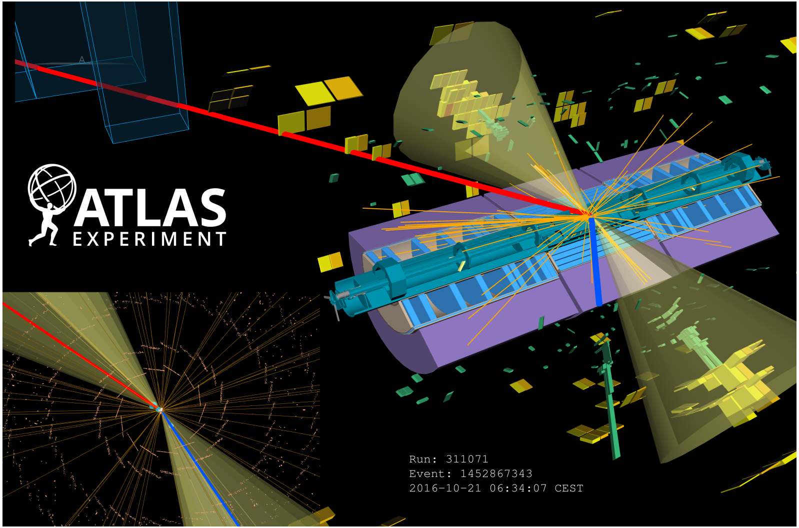

Top-antiptop candidate event reconstructed with one electron, one muon and two b-tag jets, recorded in 2016 by ATLAS at $\sqrt{s} = 13\ \mathrm{TeV}$. The jets are represented by the two yellow cones.

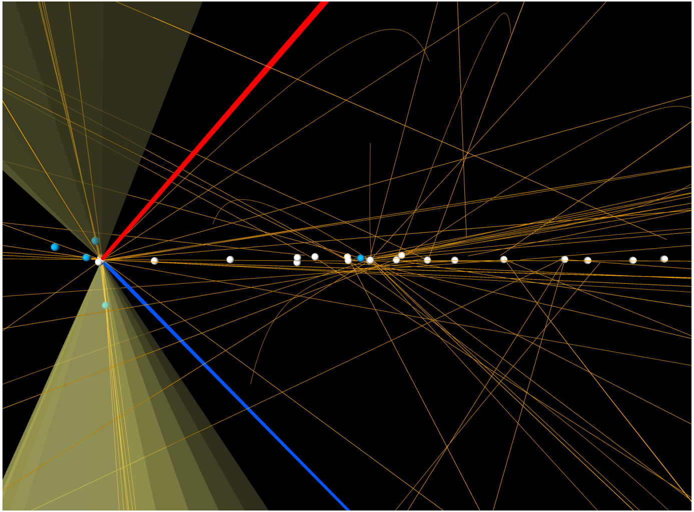

The same $t\bar{t}$ event with a zoom on the pp interaction region. The golden dots represent hits in the four layers of the pixel detector. The inner most layer (the insertable B layer) is at a radius of 3.34 cm from the beam line. The white disks represent primary vertices, and the azure ones vertices compatible with a B-decay.

The b-quark jets are identified from the tagging of secondary vertices.

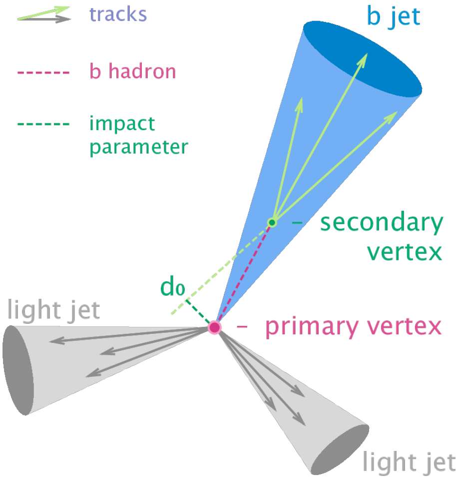

When produced in high-energy collisions they form B-hadrons. With their relatively long lifetime $(1.5 \times 10^{-12}\ \mathrm{s})$, combined with the Lorentz time-dilation factor, B-hadrons travel on average a few millimeters before decaying.

Therefore, the experimental signature for a b-quark is a jet of particles emerging from the point of the collision (the primary vertex) and a secondary vertex from the b-quark decay which is displaced from the primary vertex by several millimeters.

The decays of B-hadrons often produce more than one charged particle.

The remaining jets have to be associated to the W-boson decay(s), as indicated below

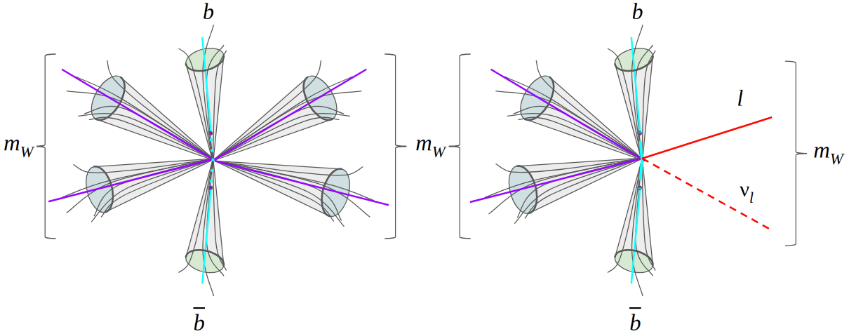

As a consequence of the unknown momentum of the $t\bar{t}$ system in the beam (z) direction, there is insufficient information to fully reconstruct the neutrino momentum in observed $t\bar{t}$ with charged lepton production.

However, the invariant mass of the two jets associated with a W boson and the invariant mass of the lepton and neutrino both can be constrained to m_W within $\pm\Gamma_W$.

The top quark mass has been determined by both the CDF and D0 collaborations at Tevatron using the measured four-momenta of the jets and leptons in observed $t\bar{t} \to 6$ jets and $t\bar{t} \to jets + \ell + \nu$ events.

Next page: an example showing the reconstructed top mass distribution from an analysis of data recorded by the CDF experiment.

Whilst the reconstructed mass peak is relatively broad due to experimental resolution, a clear peak is observed allowing the top mass to be determined with a precision of O(1%).

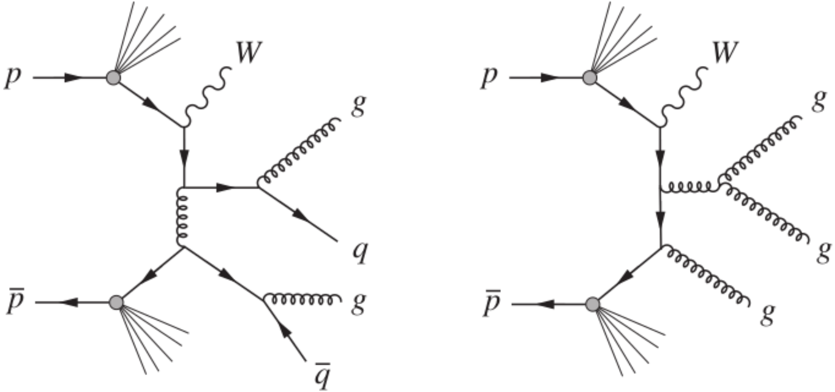

Figure 13: Background processes mimicking the top-pair quark production. The quarks and gluons are observed as jets.

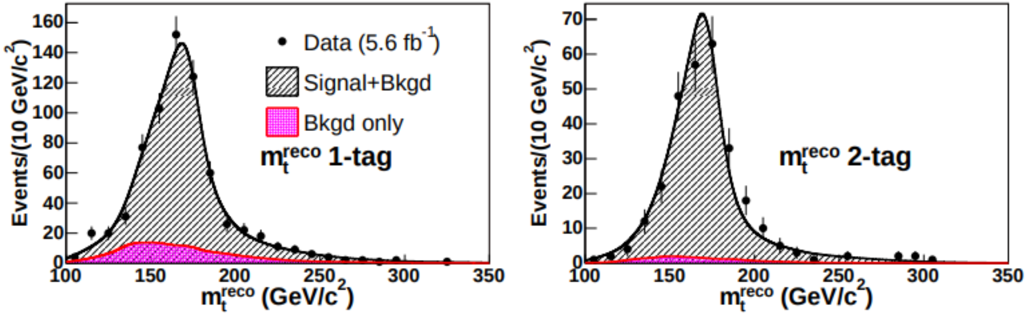

Figure 14: Distributions of the reconstructed top mass in selected $t\bar{t} \to 4$ jets $+ \ell + \nu$ events in the CDF detector at the Tevatron. Ref.: CDF 2011, arXiv:1105.0192.

The current average of the top quark mass and width measurements from the CDF and D0 experiments is

$$m_t = 173.5 \pm 1.0 \text{ GeV} \qquad \Gamma_t = 2.0 \pm 0.6 \text{ GeV} \tag{78}$$

The top width is determined much less precisely than the top quark mass because the width of the distribution above is dominated by the experimental resolution.

$t\bar{t}$ cross section

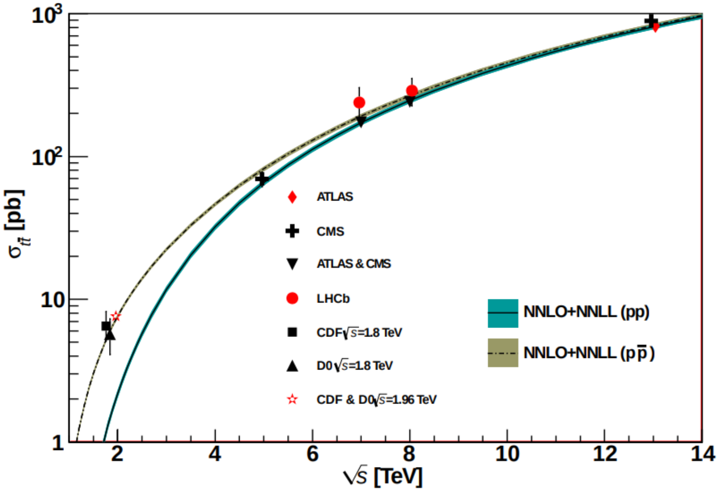

Measured and predicted $t\bar{t}$ production cross sections from Tevatron and LHC energies in $p\bar{p}$ and pp collisions, respectively. Theory curves and uncertainties are generated assuming $m_t = 172.5\ \mathrm{GeV}$.

A distinctly different process is the production of single top quarks via weak interaction.

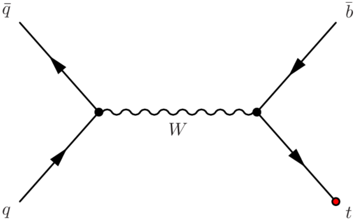

Figure 15: s-channel

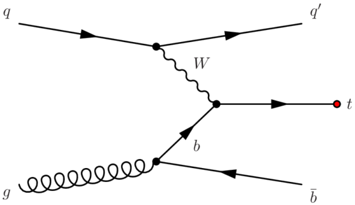

Figure 16: t-channel

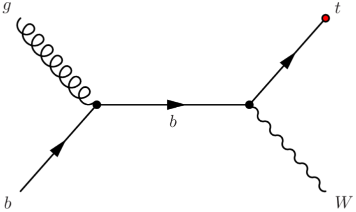

Figure 17: Wt-channel

The main significance of measuring these production processes is that their frequency is directly proportional to the $|V_{tb}|^2$ component of the CKM matrix.

The first evidence for these processes was published by the D0 collaboration in December 2006, and in March 2009 the CDF and D0 collaborations.

At the LHC, the t-channel cross section is expected to be more than 3 times as large as s-channel and Wt production, combined.

Both ATLAS and CMS have measured single top production cross sections at $\sqrt{s} = 7,\ 8,\ 13\ \mathrm{TeV}$ pp collisions assuming $m_t = 172.5\ \mathrm{GeV}$.

$t\bar{t}$ cross section

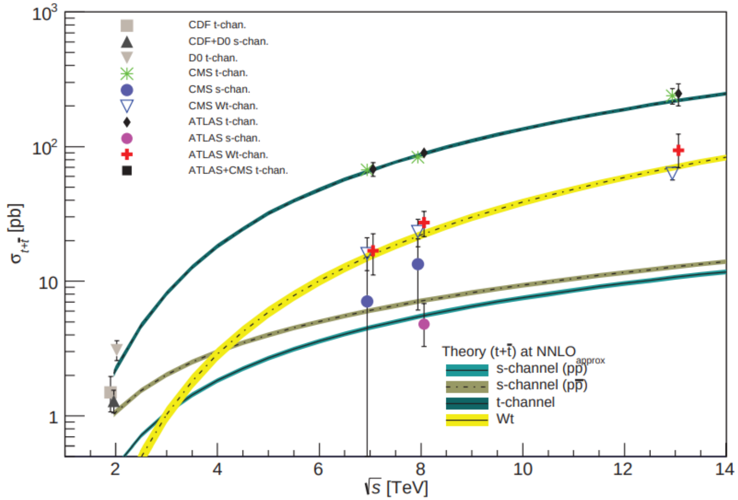

Measured and predicted single top production cross sections from Tevatron (at $\sqrt{s} = 1.96$ TeV) and LHC energies in $p\bar{p}$ and pp collisions, respectively. Ref.: PDG Reviews, 2017.

m_W Vs. m_t

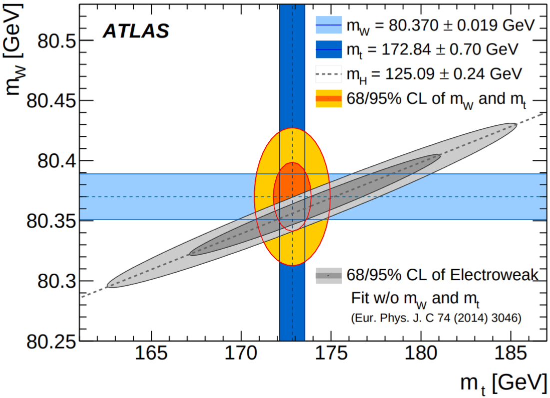

The determination from the electroweak fit uses as input the LHC measurement of the Higgs-boson mass, $m_H = 125.09 \pm 0.24$ GeV. Ref.: ATLAS 2017, arXiv:1701.07240v1.

The 68% and 95% confidence-level contours of the m_W and m_T indirect determination from the global electroweak fit of arXiv:1407.3792 are compared to the 68% and 95% confidence-level contours of the ATLAS measurements of the top-quark and W-boson masses.

Synopsis

Measurements of the differential and double-differential Drell-Yan cross sections at hadron collider show very good agreement with theoretical predictions.

The top quark is the most massive of all observed elementary particles;

- it interacts primarily by the strong interaction, but can only decay through the weak force.
- it predominantly decays to a W boson and either a bottom quark
- its lifetime is about $\sim 1/20$ of the timescale for strong interactions, and therefore it does not form hadrons

Because the top quark is so massive, the properties of the top quark allow predictions to be made of the coupling to the Higgs boson and deviations from the SM predictions might be a hint for new physics.

Appendix I: Parton Distribution Functions

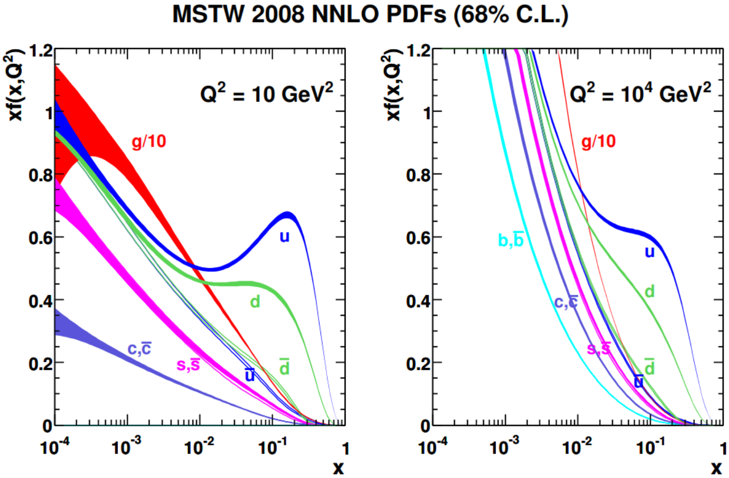

Figure 18: MSTW2008 NNLO PDF times Bjorken-x for quarks and gluons shown at a scale of $Q^2 = 10\ \mathrm{GeV}^2$ on the left and $Q^2 = 104\ \mathrm{GeV}^2$ on the right. The uncertainty of the PDFs is indicated by an uncertainty band.

Appendix II: Production cross sections

Production cross sections for various Standard Model processes as a function of the center-of-mass energy, calculated to NLO accuracy in perturbative QCD. The right axis shows the number of events expected per second at an instantaneous luminosity of $10^{33}\mathrm{cm}^{-1}\mathrm{s}^{-1}$.

As can be seen, the total Z production cross section at a collision energy of 7 TeV is 3~ 20 nb. The branching fraction of the decay $Z \to \mu^+\mu^-$ is $\sim 3.366\%$, which gives a cross-section of ~ 1 nb for the inclusive decay mode $Z \to \mu^+\mu^- + X$, where X represents any other final state particle/s, such as jets.

Ref.:arXiv:hep-ph/0611148.

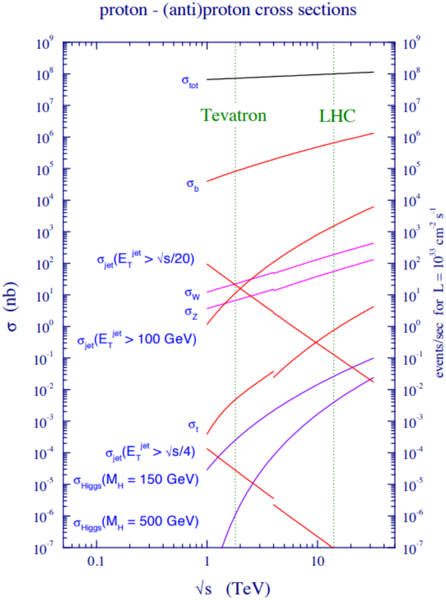

Appendix III: Drell-Yan Z

Flavor decomposition of Drell-Yan Z production as a function of the center-of-mass energy. The vertical lines indicate contributions at the Tevatron energy of 1.96 TeV and the LHC design energy of 14 TeV.

At 7 TeV, $u\bar{u}$ and $d\bar{d}$ each contribute about 40% to the leading-order process. Contributions from $s\bar{s}$ and $c\bar{c}$ are about 15% and 5%, respectively.

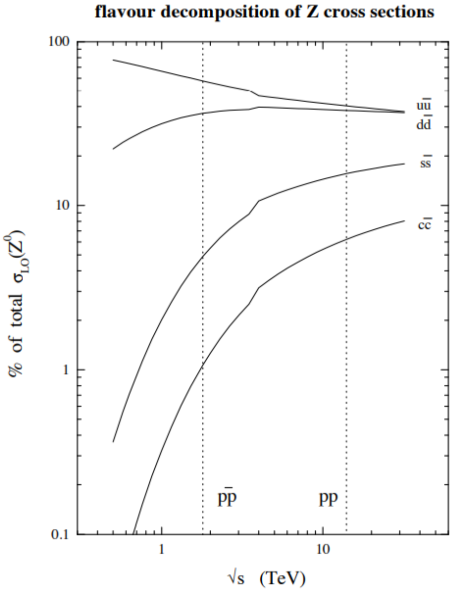

Appendix IV: Chirality states

The helicity eigenstates for a fermion/antifermion for $E \gg m$, $E \simeq |\mathbf{p}|$, are

$$u_{\uparrow} = \sqrt{E}\begin{pmatrix} +\cos\frac{\theta}{2} \\ +e^{i\phi}\sin\frac{\theta}{2} \\ +\cos\frac{\theta}{2} \\ +e^{i\phi}\sin\frac{\theta}{2} \end{pmatrix} \quad v_{\uparrow} = \sqrt{E}\begin{pmatrix} +\sin\frac{\theta}{2} \\ -e^{i\phi}\cos\frac{\theta}{2} \\ -\sin\frac{\theta}{2} \\ +e^{i\phi}\cos\frac{\theta}{2} \end{pmatrix} \tag{79}$$

$$u_{\downarrow} = \sqrt{E}\begin{pmatrix} -\sin\frac{\theta}{2} \\ +e^{i\phi}\cos\frac{\theta}{2} \\ +\sin\frac{\theta}{2} \\ -e^{i\phi}\cos\frac{\theta}{2} \end{pmatrix} \quad v_{\downarrow} = \sqrt{E}\begin{pmatrix} +\cos\frac{\theta}{2} \\ +e^{i\phi}\sin\frac{\theta}{2} \\ +\cos\frac{\theta}{2} \\ +e^{i\phi}\sin\frac{\theta}{2} \end{pmatrix} \tag{80}$$

For particles/antiparticles traveling in the z-direction, $p_z = \pm|\mathbf{p}|$, the spinors are ($\hat{S}_z$ eigenstates)

$$u_1 = N\begin{pmatrix} 1 \\ 0 \\ \frac{\pm|\mathbf{p}|}{E+m} \\ 0 \end{pmatrix},\ u_2 = N\begin{pmatrix} 0 \\ 1 \\ 0 \\ \frac{\mp|\mathbf{p}|}{E+m} \end{pmatrix},\ v_1 = N\begin{pmatrix} \frac{\pm|\mathbf{p}|}{E+m} \\ 0 \\ 1 \end{pmatrix},\ u_2 = N\begin{pmatrix} \frac{\pm|\mathbf{p}|}{E+m} \\ 0 \\ 1 \\ 0 \end{pmatrix},\ N = \sqrt{E+m} \tag{81}$$

Appendix V: Gamma matrices

In Dirac representation, the four contravariant gamma matrices are

$$\gamma^0 = \begin{pmatrix} 1 & 0 & 0 & 0 \\ 0 & 1 & 0 & 0 \\ 0 & 0 & -1 & 0 \\ 0 & 0 & 0 & -1 \end{pmatrix}, \qquad \gamma^1 = \begin{pmatrix} 0 & 0 & 0 & 1 \\ 0 & 0 & 1 & 0 \\ 0 & -1 & 0 & 0 \\ -1 & 0 & 0 & 0 \end{pmatrix} \tag{82}$$

$$\gamma^2 = \begin{pmatrix} 0 & 0 & 0 & -i \\ 0 & 0 & i & 0 \\ 0 & i & 0 & 0 \\ -i & 0 & 0 & 0 \end{pmatrix}, \qquad \gamma^3 = \begin{pmatrix} 0 & 0 & 1 & 0 \\ 0 & 0 & 0 & -1 \\ -1 & 0 & 0 & 0 \\ 0 & 1 & 0 & 0 \end{pmatrix}. \tag{83}$$

γ^0 is the time-like matrix and the other three are space-like matrices.

Appendix VI: Massive boson polarization states

For a W boson at rest, $E_W = m_W$, $p_Z \to 0$, the three possible polarization states of

$$\epsilon_-^\mu = +\frac{1}{\sqrt{2}}\,(0,\,1,\,-i,\,0) \quad \text{for} \quad S_z = -1 \tag{84}$$

$$\epsilon_0^\mu = +\frac{1}{m_W}\,(p_z,\,0,\,0,\,E_W) \quad \text{for} \quad S_z = 0 \tag{85}$$

$$\epsilon_+^\mu = -\frac{1}{\sqrt{2}}\,(0,\,1,\,+i,\,0) \quad \text{for} \quad S_z = +1 \tag{86}$$

become

$$\epsilon_-^\mu = +\frac{1}{\sqrt{2}}\,(0,\,1,\,-i,\,0) \tag{87}$$

$$\epsilon_0^\mu = (0,\,0,\,0,\,1) \tag{88}$$

$$\epsilon_+^\mu = -\frac{1}{\sqrt{2}}\,(0,\,1,\,+i,\,0) \tag{89}$$